# Maximum Available Power of Undersea Capacitive Coupling in a Wireless Power Transfer System

Hussein Mahdi[1], Bjarte Hoff[2], and Trond Østrem[3]
Department of Electrical Engineering, UiT - The Arctic University of Norway, Narvik, Norway
[1] hussein.al-sallami@uit.no, [2] bjarte.hoff@uit.no, and [3] trond.ostrem@uit.no

***Abstract*— This paper studies the maximum available power of a dissipative capacitive power transfer (CPT) system submerged in seawater. The CPT system's maximum power capability is driven using the network theory, precisely the conjugate-image approach. The equations of the maximum available load power and the system's corresponding efficiency are expressed as a function of the capacitive coupling parameters. The experimental results demonstrate that the maximum available power and the corresponding efficiency decreases by a maximum of 10%, which occurs at 1.4 MHz, when the plates' separation distance change from 100 mm to 300 mm. Besides, the system has higher power transfer capability and higher efficiency at a low-frequency range than a high one. The maximum available load power decreases by about 22.5% when increasing the frequency from 300 kHz to 1.4 MHz. Thus, the CPT system can provide a good solution to charge electric ships and underwater vehicles over a wide separation distance and low-frequency range.**

***Index Terms*—Wireless power transmission, Couplings, Impedance matching, and Network theory.**

## I. Introduction

A capacitive power transfer (CPT) system transfers power across coupling plates based on the alternating electric field principle. The CPT system is an attractive wireless power transfer option because it has a simple structure, low cost and weight, low electromagnetic interference (EMI), low ability to penetrate through metals, and good misalignment performance [1], [2]. Due to these intrinsic features, CPT has been proposed for electric vehicles [3], [4], underwater vehicles [5]–[7], and ships charging applications [8], [9].

One way to model the capacitive coupling plates (couplers) is an equivalent $\pi$ model [4], [10]. Based on this model, the maximum available efficiency of a CPT system is investigated using the coupling coefficient ($k$), the quality factor ($Q$), and their extended product ($kQ$) [11]. The investigation is later extended to include three possible solutions, namely, (1) the one that maximizes the efficiency, (2) one that maximizes the transferred power, and (3) one that realizes power matching [12], [13].

The previous solutions are analyzed for a nondissipative CPT system, in which a direct coupling with a lossless dielectric is considered. However, if a CPT system is submerged in seawater to enhance the coupling capacitance of the plates, then the seawater's dielectric losses cannot be neglected. The high percentage of the dissolved ions increase the electric conductivity and the losses of the water. Thus, the analysis for a dissipative system is needed.

The maximum available CPT system's efficiency has been previously considered for a dissipative system in [14]. The study uses the conjugate-impedance approach to drive the maximum efficiency for the CPT system submerged in seawater. Similarly, this paper addresses the conjugate-impedance analysis to achieve the maximum available power solution for a dissipative CPT system.

The maximum available load power and overall system efficiency are expressed using the coupling parameters. The paper experimentally utilised the derived equations over a 100 to 300 $\mathrm{mm}$ separation distance, and in $300\,\mathrm{kHz}$ to $1.5\,\mathrm{MHz}$ operating frequency. The rest of the paper is organized as follows: Section II provides the theoretical analysis. Section III presents the experimental results and discussion. The conclusion is drawn in section IV.

## II. Theoretical Analysis

A CPT system can be modelled using both the $\pi$ model and its equivalent linear two-port network, as shown in Fig. 1. The two-port network representation is considered to make a general formulation for the CPT scheme. In this representation, the couplers are considered as a black box from which only the voltages $(u_1, u_2)$ and the currents $(i_1, i_2)$ can be measured. The voltage-to-current relation can be expressed through an admittance matrix:

$$\begin{bmatrix} i_1 \\ i_2 \end{bmatrix} = \begin{bmatrix} Y_{\mathrm{I}} & -Y_{\mathrm{M}} \\ -Y_{\mathrm{M}} & Y_{\mathrm{II}} \end{bmatrix} \begin{bmatrix} u_1 \\ u_2 \end{bmatrix}, \tag{1}$$

where $Y_{\mathrm{I}}$ and $Y_{\mathrm{II}}$ are the self-admittance coefficients, and $Y_{\mathrm{M}}$ is the mutual admittance coefficient, which can be expressed as:

$$\begin{cases} Y_{\mathrm{I}} & = \overbrace{(G_1 + G_{\mathrm{M}})}^{G_{\mathrm{I}}} + \mathrm{j}\overbrace{(B_1 + B_{\mathrm{M}})}^{B_{\mathrm{I}}} \\ Y_{\mathrm{M}} & = G_{\mathrm{M}} + \mathrm{j}B_{\mathrm{M}} \\ Y_{\mathrm{II}} & = \underbrace{(G_2 + G_{\mathrm{M}})}_{G_{\mathrm{II}}} + \mathrm{j}\underbrace{(B_2 + B_{\mathrm{M}})}_{B_{\mathrm{II}}} \end{cases}, \tag{2}$$

where $(G)$ is the conductance, $(B = \omega C)$ is the susceptance parts of the admittance, and $\omega$ is the angular frequency. The admittance matrix $Y$ can be calculated from the scattering matrix $S$:

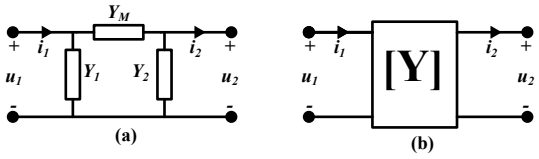


Fig. 1. Network representation of CPT: (a) A $\pi$ model. (b) A linear two-port network.

$$\begin{aligned} Z &= Z_o(I-S)^{-1}(I+S) \\ Y &= Z^{-1} \end{aligned}, \tag{3}$$

where $Y = \left[\begin{smallmatrix} Y_{\mathrm{I}} & -Y_{\mathrm{M}} \\ -Y_{\mathrm{M}} & Y_{\mathrm{II}} \end{smallmatrix}\right]$, $S = \left[\begin{smallmatrix} S_{11} & S_{12} \\ S_{21} & S_{22} \end{smallmatrix}\right]$, and $Z_o$ is the reference admittance which has a real positive value and is practically chosen to be $50\,\Omega$.

Fig. 2(a) shows the connection of the two-port network to transmitter and receiver external circuits. The input admittance $Y_{\mathrm{in}}$, as seen by the transmitter side, is expressed as:

$$Y_{\mathrm{in}} = Y_{\mathrm{I}} - \frac{Y_{\mathrm{M}}^2}{Y_{\mathrm{II}} + Y_{\mathrm{L}}} \tag{4}$$

where $Y_{\mathrm{L}} = G_L + \mathrm{j}B_L$ is the load admittance. The source circuit ($i_{\mathrm{s}}$ and $Y_{\mathrm{S}} = G_S + \mathrm{j}B_S$) is replaced by its Norton equivalent at the receiver side, as illustrated in Fig. 2(b). The Norton equivalent can be expressed as:

$$Y_{\mathrm{N}} = Y_{out} = Y_{\mathrm{II}} - \frac{Y_{\mathrm{M}}^2}{Y_{\mathrm{I}} + Y_{\mathrm{S}}}, \tag{5}$$

$$i_{\mathrm{N}} = \frac{-Y_{\mathrm{M}}}{Y_{\mathrm{I}} + Y_{\mathrm{S}}} i_{\mathrm{s}}. \tag{6}$$

The input admittance can be considered as the conjugate of the source admittance ($Y_{\mathrm{in}} = Y_{\mathrm{S}}^*$) and the output admittance is the conjugate of the load admittance ($Y_{out} = Y_{\mathrm{L}}^*$), based on the conjugate-image theorem [15]. If the network is nondissipative, then (4) and (5) are identical. However, for a dissipative network, (4) and (5) can be solved for $Y_{\mathrm{S}}$ and $Y_{\mathrm{L}}$. The following two expressions can be introduced to clearing the fraction term in both (4) and (5):

$$\theta_{\mathrm{G}} = \frac{G_{\mathrm{s}}}{G_{\mathrm{I}}} = \frac{G_{\mathrm{L}}}{G_{\mathrm{II}}} \tag{7a}$$

$$\theta_{\mathrm{B}} = \frac{B_{\mathrm{s}} + B_{\mathrm{I}}}{G_{\mathrm{I}}} = \frac{B_{\mathrm{L}} + B_{\mathrm{II}}}{G_{\mathrm{II}}} \tag{7b}$$

The expressions $\theta_{\mathrm{G}}$ and $\theta_{\mathrm{B}}$ are defined in [15] as intermediate variables, but their physical meanings are not given. The source and load admittance can be rewritten as:

$$Y_{\mathrm{S}} = G_{\mathrm{I}}\left(\theta_{\mathrm{G}} + \mathrm{j}\theta_{\mathrm{B}}\right) - \mathrm{j}B_{\mathrm{I}} \tag{8a}$$

$$Y_{\mathrm{L}} = G_{\mathrm{II}}\left(\theta_{\mathrm{G}} + \mathrm{j}\theta_{\mathrm{B}}\right) - \mathrm{j}B_{\mathrm{II}} \tag{8b}$$

While the mutual admittance term can be expressed as:

$$Y_{\mathrm{M}}^2 = G_{\mathrm{I}}\,G_{\mathrm{II}}\left(1 - \theta_{\mathrm{G}} + \mathrm{j}\theta_{\mathrm{B}}\right)\left(1 + \theta_{\mathrm{G}} + \mathrm{j}\theta_{\mathrm{B}}\right) \tag{9}$$

From (9), the two expressions ($\theta_{\mathrm{G}}$ and $\theta_{\mathrm{B}}$) can be redefined.

$$\theta_{\mathrm{G}} = \sqrt{\left(1 - \frac{G_{\mathrm{M}}^2}{G_{\mathrm{I}}\,G_{\mathrm{II}}}\right)\left(1 + \frac{B_{\mathrm{M}}^2}{G_{\mathrm{I}}\,G_{\mathrm{II}}}\right)} \tag{10a}$$

$$\theta_{\mathrm{B}} = \frac{G_{\mathrm{M}}\,B_{\mathrm{M}}}{G_{\mathrm{I}}\,G_{\mathrm{II}}} \tag{10b}$$

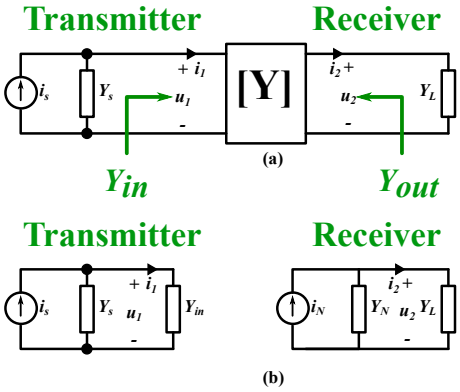


Fig. 2. A general representation of CPT system: (a) Two-port network connected to source and load. (b) The transmitter and receiver equivalent circuits.

The input ($P_{\mathrm{in}}$) and output power ($P_{\mathrm{L}}$) can be expressed as:

$$\begin{aligned} P_{\mathrm{in}} &= \frac{1}{2}\mathrm{Re}(Y_{\mathrm{in}} + Y_{\mathrm{S}})|u_1|^2 = \frac{1}{2}\frac{\mathrm{Re}(Y_{\mathrm{in}} + Y_{\mathrm{S}})|i_{\mathrm{s}}|^2}{|Y_{\mathrm{S}} + Y_{\mathrm{in}}|^2} \\ &= \frac{1}{2}\frac{\mathrm{Re}(Y_{\mathrm{in}} + Y_{\mathrm{S}})|Y_{\mathrm{II}} + Y_{\mathrm{L}}|^2|i_{\mathrm{s}}|^2}{|\left(Y_{\mathrm{II}} + Y_{\mathrm{L}}\right)\left(Y_{\mathrm{S}} + Y_{\mathrm{in}}\right)|^2} \end{aligned} \tag{11}$$

$$\begin{aligned} P_{\mathrm{L}} &= \frac{1}{2}\mathrm{Re}(Y_L)|u_2|^2 = \frac{1}{2}\frac{\mathrm{Re}(Y_{\mathrm{L}})|i_{\mathrm{N}}|^2}{|Y_{\mathrm{N}} + Y_{\mathrm{L}}|^2} \\ &= \frac{1}{2}\frac{\mathrm{Re}(Y_{\mathrm{L}})|Y_{\mathrm{M}}|^2|i_{\mathrm{s}}|^2}{|\left(Y_{\mathrm{N}} + Y_{\mathrm{L}}\right)\left(Y_{\mathrm{I}} + Y_{\mathrm{S}}\right)|^2} \end{aligned} \tag{12}$$

where $\mathrm{Re}(\,)$ is the real part of the complex expression. The maximum available power by the source is achieved when $Y_{\mathrm{in}} = Y_{\mathrm{S}}^*$, and it can be calculated as:

$$P_{\mathrm{s,max}} = \frac{1}{2}\frac{G_{\mathrm{s}}|i_{\mathrm{s}}|^2}{|\left(Y_{\mathrm{in}} + Y_{\mathrm{S}}\right)|^2} = \frac{1}{8}\frac{|i_{\mathrm{s}}|^2}{G_{\mathrm{in}}} \tag{13}$$

Defining the following two parameters for the convenience of mathematical symbols:

$$\psi^2 = \frac{G_{\mathrm{M}}^2}{G_{\mathrm{I}}\,G_{\mathrm{II}}} \tag{14a}$$

$$\chi^2 = \frac{B_{\mathrm{M}}^2}{G_{\mathrm{I}}\,G_{\mathrm{II}}} \tag{14b}$$

$\psi$ represents the ratio between the coupling and the self-conductance. $\chi$ is an equivalent to the quality factor. Similarly, the maximum available power derived to the load by Norton-equivalent circuit is achieved when $Y_{\mathrm{N}} = Y_{\mathrm{L}}^*$. The maximum available load power can be calculated from (12) and (14) as follows.

$$P_{\mathrm{L,max}} = P_{\mathrm{s,max}}\frac{\psi^2 + \chi^2}{\left(1 + \theta_{\mathrm{G}}\right)^2 + \theta_{\mathrm{B}}^2} \tag{15}$$

For a nondissipative network and lossless source, that is $\psi = 0$ and $G_s = 0$ respectively, the maximum available power becomes:

$$P_{\mathrm{L,max}} = P_{\mathrm{s,max}}\frac{\chi^2}{\left(1 + \chi^2\right)} \tag{16}$$

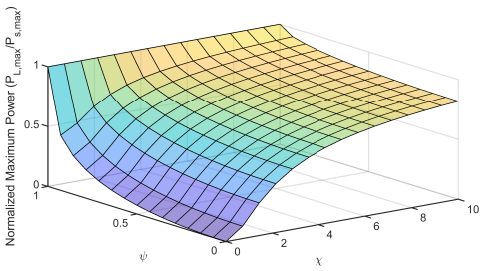


Fig. 3. The theoretical maximum available power calculated from (15).

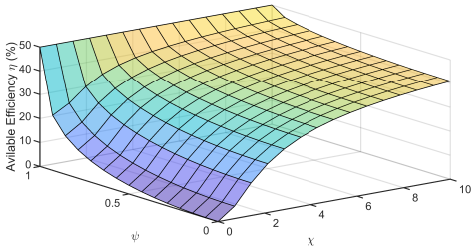


Fig. 4. The theoretical available efficiency at maximum power transfer calculated from (17).

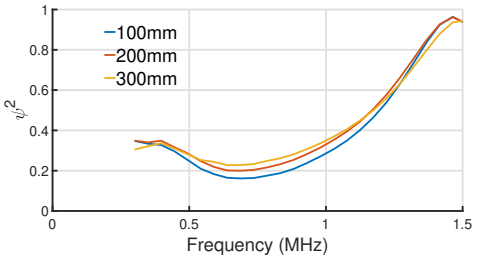


Fig. 6. The measured $\psi^2$ versus frequency

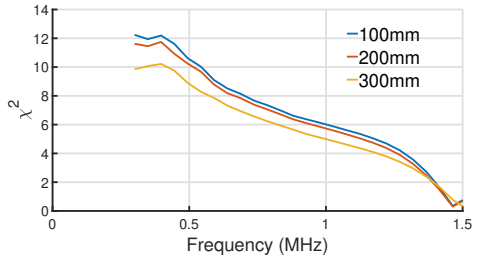


Fig. 7. The measured $\chi^2$ versus frequency

which is the same equation that reported in [12]. From (11) (12), the available efficiency at maximum power transfer of CPT system is given as:

$$\eta = \frac{P_{\mathrm{L}}}{P_{\mathrm{in}}} = \frac{1}{2}\frac{\psi^2 + \chi^2}{(1+\theta_{\mathrm{G}})^2 + \theta_{\mathrm{B}}^2} \tag{17}$$

For a nondissipative network and lossless source, the efficiency becomes:

$$\eta = \frac{1}{2}\frac{\chi^2}{(1+\chi^2)} \tag{18}$$

From (15) and as illustrated in Fig. 3, when $\chi$ and $\psi$ increases, the maximum available load power increases to reach the $P_{\mathrm{s,max}}$. Likewise, from (17) when $\chi$ and $\psi$ increases, the maximum efficiency of the CPT system reaches 50%, as shown in Fig 4. For a nondissipative CPT system and from (16) and (18), as asymptotically $\chi \to \infty$ provides $P_{L,max} \to P_{s,max}$ and $\eta \to 50\%$, respectively.

## III. Experimental Results and Discussion

Two pairs of square-shaped electrodes of 6082 aluminium sheets covered with a plastic lamination pouch for isolation were used to realize the couplers. A PicoVNA Vector Network Analyzers is used in the measurements, as illustrated in Fig. 5. The measurement is carried out over a distance (d) from $100\,\mathrm{mm}$ to $300\,\mathrm{mm}$ and a frequency range from $300\,\mathrm{kHz}$ to $1.5\,\mathrm{MHz}$ in seawater that is collected from the local harbour.

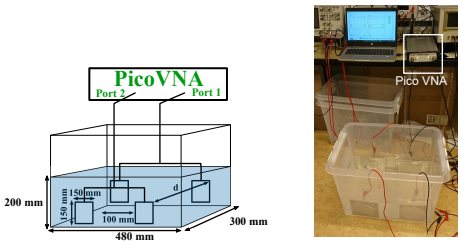


Fig. 5. The measurement setups

The two coefficients $\psi^2$ and $\chi^2$ are measured using (14). Fig. 6 shows that the $\psi^2$ cannot be neglected over the frequency range. Thus, if the nondissipative analysis is used, then imprecise results are achieved. The increase of $\psi^2$ the increase of the ions' mobility in the seawater. When the frequency of the electric fields increases, the coupling conductivity and hence $\psi^2$ also increases.

Fig. 7 shows that $\chi^2$ monotonically decreases with the increase of frequency. This coefficient is asymptotically approaching zero around $1.5\,\mathrm{MHz}$, which is the self-resonant frequency of the couplers (at which $C_M \to 0$ and $\chi^2 \to 0$). The maximum rates of change of $\psi^2$ and $\chi^2$ are 42% at $736.5\,\mathrm{kHz}$ and 24% at $736.5\,\mathrm{kHz}$, respectively, when the separation distance is increased from $100\,\mathrm{mm}$ to $300\,\mathrm{mm}$.

According to (15) and (17), the CPT system is expected to give higher power transfer capability and better efficiency at lower frequency ranges than at higher ones. Fig. 8 depicts the maximum load power, which is plotted using the measured values of $\psi^2$ and $\chi^2$ and into (15) and (16). The results show that at low frequencies, more power can be transferred than at higher ones. For example, the maximum power that can be transferred to the load at $100\,\mathrm{mm}$ separation distance decreases from about 86% of the maximum source power at $300\,\mathrm{kHz}$ to about 57% at $1.5\,\mathrm{MHz}$.

The results also demonstrate that the change of the separation distance has almost a negligible effect on the maximum power transfer capability. The maximum available power decreases by a maximum of 10% at 1.4 MHz when the

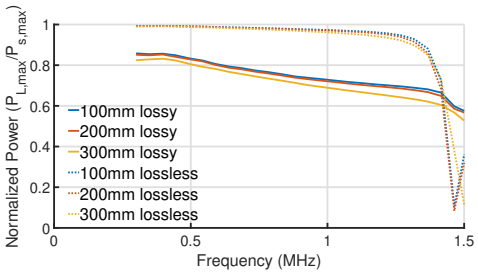


Fig. 8. The normalized power for lossy (15) and lossless (16) CPT system versus frequency.

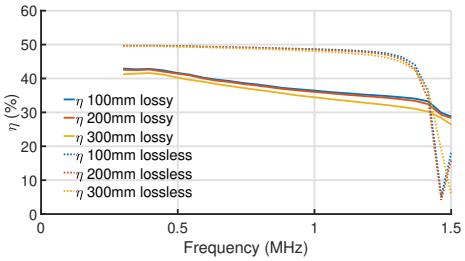


Fig. 9. The efficiency for lossy (17) and lossless (18) CPT system versus frequency at maximum power transfer.

plates' separation distance change from 100 mm to 300 mm. Moreover, the analysis for a nondissipative system gives overestimated results compared to the analysis for the dissipative one, except when approaching 1.5 MHz. The maximum available load power decreases by about 22.5% when increasing the frequency from 300 kHz to 1.4 MHz.

The available efficiency of the CPT system, from (17) and (18), is also investigated over the frequency and distance ranges at maximum power transfer. Fig 9 illustrates that the nondissipative analysis gives overestimated values compared to the dissipated analysis. Similar to maximum available power, the separation distance has a negligible effect on the efficiency. Besides, the system has higher efficiencies at a low-frequency range than at a higher one. At 100 mm distance, for instance, the CPT system's efficiency decreases from about 43% at 300 kHz to about 28% at 1.5 MHz.

## IV. Conclusion

This paper investigates a dissipative capacitive power transfer (CPT) system submerged in seawater using the conjugate-image approach to drive the maximum available power. The maximum available load power and the corresponding efficiency have been expressed as functions of capacitive coupling parameters. The experimental results show that the maximum available power and the corresponding efficiency of the system decrease maximum by 10% when the plates' separation distance change from 100 mm to 300 mm.

The system has higher power transfer capability and efficiency at low frequencies than at higher ones.When increasing the frequency from 300 kHz to 1.4 MHz, the maximum available power decreases by about 22.5%. Unlike in the case of air-gapped CPT systems, which require high frequency to increase their power transfer capabilities, seawater CPT systems can operate at low frequencies to transfer high power with low EMI problem. Higher efficiency can also be achieved if the maximum power transfer is not considered as in [14]. Based on the analysis, the CPT system can provide an attractive wireless charging solution to electric ships and underwater vehicles with a wide separation distance and low-frequency range.

## References


[1] F. Lu, H. Zhang, and C. Mi, "A Review on the Recent Development of Capacitive Wireless Power Transfer Technology," *Energies*, vol. 10, no. 11, p. 1752, nov 2017.

[2] L. Huang, A. P. Hu, A. Swain, S. Kim, and Y. Ren, "An overview of capacitively coupled power transfer - A new contactless power transfer solution," *Proceedings of the 2013 IEEE 8th Conference on Industrial Electronics and Applications, ICIEA 2013*, pp. 461–465, 2013.

[3] F. Lu, H. Zhang, and C. Mi, "A Two-Plate Capacitive Wireless Power Transfer System for Electric Vehicle Charging Applications," *IEEE Transactions on Power Electronics*, vol. 33, no. 2, pp. 964–969, 2018.

[4] H. Zhang, F. Lu, H. Hofmann, W. Liu, and C. C. Mi, "A Four-Plate Compact Capacitive Coupler Design and LCL-Compensated Topology for Capacitive Power Transfer in Electric Vehicle Charging Application," *IEEE Transactions on Power Electronics*, vol. 31, no. 12, pp. 8541–8551, 2016.

[5] M. Tamura, Y. Naka, K. Murai, and T. Nakata, "Design of a Capacitive Wireless Power Transfer System for Operation in Fresh Water," *IEEE Transactions on Microwave Theory and Techniques*, vol. 66, no. 12, pp. 5873–5884, 2018.

[6] M. Tamura, Y. Naka, and K. Murai, "Design of capacitive coupler in underwater wireless power transfer focusing on kQ product," *IEICE Transactions on Electronics*, vol. E101C, no. 10, pp. 759–766, 2018.

[7] M. Urano, K. Ata, and A. Takahashi, "Study on underwater wireless power transfer via electric coupling with a submerged electrode," *IMFEDK 2017 - 2017 International Meeting for Future of Electron Devices, Kansai*, pp. 36–37, 2017.

[8] H. Zhang and F. Lu, "Feasibility Study of the High-Power Underwater Capacitive Wireless Power Transfer for the Electric Ship Charging Application," *2019 IEEE Electric Ship Technologies Symposium, ESTS 2019*, pp. 231–235, 2019.

[9] H. Mahdi, B. Hoff, and T. Ostrem, "Evaluation of Capacitive Power Transfer for Small Vessels Charging Applications," *IEEE International Symposium on Industrial Electronics*, vol. 2020-June, pp. 1605–1610, 2020.

[10] L. Huang and A. P. Hu, "Defining the mutual coupling of capacitive power transfer for wireless power transfer," *Electronics Letters*, vol. 51, no. 22, pp. 1806–1807, 2015.

[11] T. Ohira, "Extended k-Q product formulas for capacitive- and inductive-coupling wireless power transfer schemes," *IEICE Electronics Express*, vol. 11, no. 9, pp. 1–7, 2014.

[12] M. Dionigi, M. Mongiardo, G. Monti, and R. Perfetti, "Modelling of wireless power transfer links based on capacitive coupling," *International Journal of Numerical Modelling: Electronic Networks, Devices and Fields*, vol. 30, no. 3-4, 2017.

[13] J. Kracek and M. Svanda, "Power balance of capacitive wireless power transfer," *Proceedings of European Microwave Conference in Central Europe, EuMCE 2019*, vol. 7, pp. 521–524, 2019.

[14] H. Mahdi, B. Hoff, and T. Ostrem, "Maximum Available Efficiency of Undersea Capacitive Coupling in a Wireless Power Transfer System," *IEEE International Symposium on Industrial Electronics*, 2021 (accepted).

[15] S. Roberts, "Conjugate-Image Impedances," *Proceedings of the IRE*, vol. 34, no. 4, pp. 198p–204p, 1946.